Protein Transport in Ultrafiltration Hollow-Fiber Bioreactors

Anant Y. Patkar and Jürgen Koska
Biotechnology Lab. and Dept. of Chemical Engineering, University of British Columbia, Vancouver, BC V6T 1Z3, Canada

David G. Taylor
Dept. of Chemical Engineering, University of Ottawa, Ottawa, ONT K1N 6N5, Canada

Bruce D. Bowen
Dept. of Chemical Engineering, University of British Columbia, Vancouver, BC V6T 1Z2, Canada

James M. Piret
Biotechnology Lab. and Dept. of Chemical Engineering, University of British Columbia, Vancouver, BC V6T 1Z3, Canada

A 1-D model, which neglects radial variations, describes the hydrodynamics of cell-free ultrafiltration hollow-fiber bioreactors (HFBRs) and the transport of high-molecular-weight proteins trapped in the extracapillary space (ECS). The profiles of radially-averaged protein concentrations predicted by this model are identical to those obtained using a model with radial variations. The model predictions agree well with axial profiles of bovine serum albumin (BSA) and human transferrin concentrations measured in transient and steady-state experiments. The validated model explores the influence of cell culture operating conditions on HFBR protein transport. Increasing protein loading decreases BSA and transferrin polarization in HFBRs operated with unidirectional lumen flow. A relationship developed predicts the protein loading needed to ensure a nonzero steady-state protein concentration throughout the ECS. This critical protein loading depends only on the lumen pressure drop and the ECS protein osmotic pressure. Periodic reversal of the lumen flow direction also decreases protein polarization. The influence of the flow-direction switching time and membrane permeability on the ECS protein distribution is investigated.

Introduction

Immobilized mammalian-cell hollow-fiber bioreactors (HFBRs) have been used for the production of monoclonal antibodies (Altshuler et al., 1986; Evans and Miller, 1988; Heifetz et al., 1989) and hormones (Knazek et al., 1974), and as a bioartificial liver (Nyberg et al., 1993). A HFBR consists of a bundle of hollow fibers potted at both ends in epoxy and enclosed in a cylindrical casing. Cells are usually inoculated into and retained in the space between the fibers (extracapillary space or ECS). Thin sections of the reactors have revealed tissue-like cell densities in the ECS (Knazek et al., 1974). The medium flowing through the fiber lumens supplies nutrients to the cells and removes metabolic waste products such as lactate and ammonium. HFBRs thus provide a low-shear environment for the immobilized cells and permit months of continuous product synthesis (David et al., 1978; Altshuler et al., 1986; von Wedel, 1987). Ultrafiltration HFBRs concentrate high-molecular-weight products in the ECS. Antibodies, for example, have been harvested from HFBRs at over 10 g/L concentrations (Heifetz et al., 1989; Piret and Cooney, 1990) and greater than 95% purity (Heifetz et al., 1989).

The cell culture environment in the immobilized cell region is heterogeneous. Gradients in nutrients (such as glucose and oxygen), metabolites, and growth factor proteins (such as transferrin and insulin) can influence the cell metabolism and limit the scale-up of these reactors (Heath and Belfort, 1987; Piret and Cooney, 1990; Piret et al., 1991; Piret and Cooney,

Correspondence concerning this article should be addressed to J. M. Piret.

1991). A thorough understanding of the hydrodynamics and mass transport properties of HFBRs is therefore essential for optimal design and operation of these reactors.

For the typically low membrane permeabilities encountered in HFBRs, the lumen hydrostatic pressure decreases approximately linearly along the length of the reactor, while the ECS hydrostatic pressure is virtually constant. At low ECS protein concentrations, the resulting transmembrane hydrostatic pressure differences induce a secondary flow in the ECS (Tharakan and Chau, 1986; Heath et al., 1990). This convective flow transports high-molecular-weight proteins to the downstream end of the HFBR (Waterland et al., 1975). Piret and Cooney (1990) correlated the downstream polarization of growth factors with downstream hybridoma growth. They also demonstrated that periodic switching of the lumen flow direction resulted in more uniform ECS protein distribution and a two- to three-fold increase in hybridoma growth and bioreactor antibody productivity.

Several mathematical models describing the hydrodynamics in cell-free HFBRs, applicable during the first few days after inoculation when the ECS cell concentrations are low, have been developed (Bruining, 1989; Kelsey et al., 1990; Pillarella and Zydney, 1990). These models, however, did not address the issue of osmotic pressures exerted by high-molecular-weight proteins retained in the ECS by ultrafiltration membranes. Taylor et al. (1994) derived a model incorporating osmotic effects and determined the influence of ECS protein loading, membrane permeability, and lumen recycle flow rate on the ECS protein distribution.

In this article, a simplified one-dimensional (1-D) model of the hydrodynamics and protein transport in ultrafiltration HFBRs is developed whose results are virtually identical to those of the more complex, two-dimensional (2-D) model reported by Taylor et al. The protein distribution results predicted by the 1-D model are compared with experimental measurements. The model is then used to explore alternative HFBR startup strategies.

Theory

Model assumptions

Taylor et al. (1994) developed a detailed 2-D mathematical model to describe the transient fluid dynamics and protein transport in a cell-free, isotropic membrane HFBR. The extreme radius/length ratio of a representative fiber unit in most HFBRs suggested that a 1-D model could provide a sufficiently accurate representation of HFBR hydrodynamics and ECS protein redistribution. In this modified model, radial variations in ECS protein concentration as well as in ECS and lumen pressures and velocities were neglected. Such a simplification greatly reduced the problem complexity and the computation time. The simplified model is henceforth referred to as the 1-D model.

As in the 2-D model, the multifiber reactor was approximately represented by a single fiber surrounded by its associated Krogh cylinder, assuming no fluid or protein exchange with neighboring fibers. Figure 1 shows a diagram of the entire HFBR as well as the geometry of the representative Krogh cylinder. Krogh (1919) first applied this approximation to model tissue-capillary systems. Many HFBR models have used this approximation. As the fiber is rigid and the fluid incompressible, it was assumed that the fluid velocities adjust instantaneously to the time-dependent changes in osmotic pressures. The inertial terms of the Navier-Stokes equation were assumed to be negligible at the low Reynolds numbers (<10) encountered in the ECS and lumen. Transmembrane flows were assumed to occur only in the radial direction, while protein leakage through the ultrafiltration membranes was assumed to be negligible. In addition, the fluid density and viscosity, and the protein diffusivity, were assumed to be independent of protein concentration. Taylor et al. have discussed these assumptions in more detail.

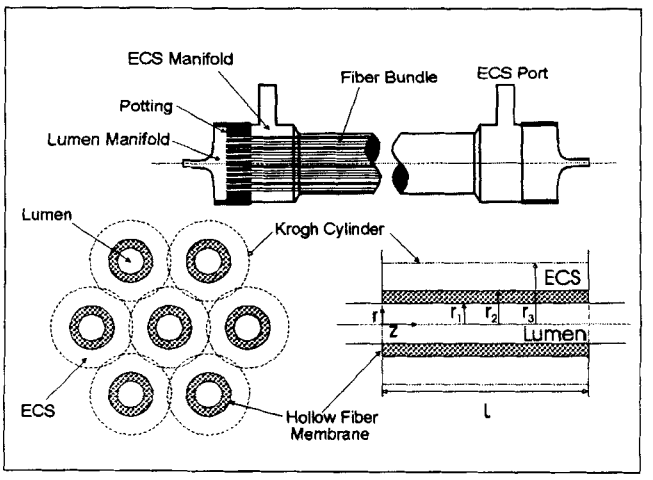

Figure 1. Hollow-fiber bioreactor geometry (top).

Cross section of the fiber bundle and Krogh cylinders associated with fibers (bottom left). Single Krogh cylinder unit showing spatial parameters of the model (bottom right).

Model equations

To describe HFBR hydrodynamics, Taylor et al. derived a second-order differential equation for the radially-averaged axial lumen velocity by performing a fluid mass balance over a differential axial volume in the lumen. It was shown that all other hydrodynamic variables, such as the radial and axial velocity components and the hydrostatic pressures in the lumen and ECS, could be related to the average lumen velocity. A similar mass balance over an ECS differential volume results in the following differential equation for the radially-averaged axial ECS fluid velocity, $\bar{u}_E$:

$$\frac{d^2\bar{u}_E(z)}{dz^2} - \frac{16L_p\xi}{r_1^3}\bar{u}_E(z) = -\frac{16L_p}{r_1(r_3^2-r_2^2)}\bar{u}_{Li} + \frac{2r_1L_p}{\mu(r_3^2-r_2^2)}\frac{d\bar{\Pi}_E}{d\bar{C}_E}\frac{d\bar{C}_E(z)}{dz} \quad (1)$$

where the geometric constant ξ is given by:

$$\xi = 1 + \frac{r_1^4}{4r_3^4\ln\left(\frac{r_3}{r_2}\right) - (r_3^2-r_2^2)(3r_3^2-r_2^2)}. \quad (2)$$

In Eqs. 1 and 2, z is the axial distance measured from the start of the permeable portion of the fibers, L_p is the membrane

Table 1. Model Parameters

$N = 8{,}128$
$r_1 = 1.00\times10^{-4}$ m (dry), 1.15×10^{-4} m (wet), 0.905×10^{-4} m (potting)
$r_2 = 1.08\times10^{-4}$ m (dry), 1.24×10^{-4} m (wet), 1.05×10^{-4} m (potting)
$r_3 = 1.75\times10^{-4}$ m
$L = 0.215$ m (dry), 0.238 m (wet)
$\mu = 0.001$ kg/m·s
$D = 7\times10^{-11}$ m^2/s
$A_2 = 10.473\times10^{-3}$ m^3/kg
$A_3 = 17.374\times10^{-6}$ m^6/kg^2
$L_p = 6\times10^{-15}$ m
$M = 69$ kDa (BSA), 77 kDa (transferrin)
$T = 293$ K

permeability, μ is the fluid viscosity, $\overline{\Pi}_E$ is the radially-averaged osmotic pressure, which is a function of the radially-averaged ECS protein concentration $\overline{C}_E$, and $\overline{u}_{Li}$ is the radially-averaged inlet velocity to each fiber lumen. The inner and outer fiber radii, and the Krogh cylinder radius are denoted by r_1, r_2, and r_3, respectively (Figure 1). Since both ECS ports are closed, Eq. 1 is subject to the following zero flux boundary conditions:

$$\overline{u}_E = 0 \quad \text{at} \quad z = 0 \tag{3}$$

$$\overline{u}_E = 0 \quad \text{at} \quad z = L \tag{4}$$

where L denotes the permeable length of the fiber bundle.

When radial concentration gradients are ignored, transient protein transport in the ECS can be described by the simplified convective-diffusion equation:

$$\frac{\partial \overline{C}_E}{\partial t} = D\frac{\partial^2 \overline{C}_E}{\partial z^2} - \frac{\partial}{\partial z}(\overline{u}_E \overline{C}_E) \tag{5}$$

where D is the protein diffusivity. The initial and boundary conditions associated with Eq. 5 indicate that the ECS protein concentration is initially homogeneous and that there is no protein transfer through either end of the ECS

$$\overline{C}_E = C_{E0} \quad \text{at} \quad 0 \le z \le L, \quad t = 0 \tag{6}$$

$$\frac{\partial \overline{C}_E}{\partial z} = 0 \quad \text{at} \quad z = 0, \quad t \ge 0 \tag{7}$$

$$\frac{\partial \overline{C}_E}{\partial z} = 0 \quad \text{at} \quad z = L, \quad t \ge 0. \tag{8}$$

Bovine serum albumin (BSA) and human transferrin were used as test proteins for experimentally investigating ECS protein redistribution. The osmotic pressure of BSA was related to its concentration by a simple virial equation of the form:

$$\Pi = \frac{RT}{M}(C + A_2C^2 + A_3C^3) \tag{9}$$

where R represents the universal gas constant, T is the absolute temperature, and M is the protein molecular weight. The two virial coefficients, A_2 and A_3, were obtained by fitting Eq. 9 to the pH 6.6–8.2 osmotic pressure data reported by Scatchard et al. (1946a,b). The fitted parameters are listed in Table 1. Equation 9 differs from the correlation developed by Vilker et al. (1981) for pH 7.4, but as Figure 2 shows, it better represents the osmotic pressure data for the range of BSA concentrations of interest to this study. For cases in which only transferrin was added to the ECS, the osmotic pressure was assumed to be given by the ideal osmotic pressure relationship, that is, Eq. 9 with the virial coefficients, A_2 and A_3, set to zero. This is a reasonable assumption at the low concentrations (<1 g/L) used in the transferrin distribution experiments. In the BSA/transferrin loading experiments, the transferrin content was less than 0.2% of the total protein concentration. For model comparison with these cases, it was therefore assumed that transferrin contributed negligibly to the ECS osmotic pressure.

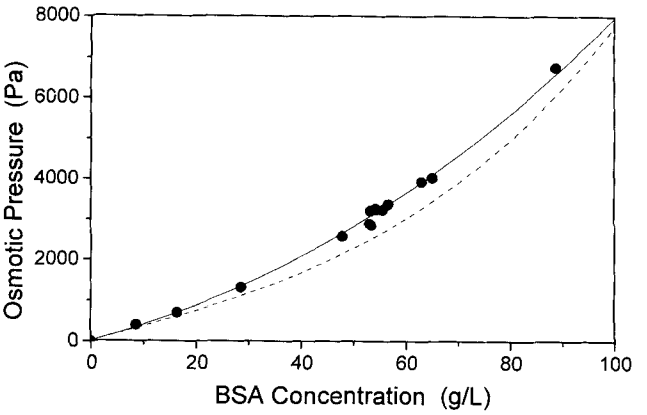

Figure 2. Comparison of osmotic pressure correlations.
(●) Experimental data by Scatchard et al. (1946a,b); (—) fitted equation; (- -) equation of Vilker et al. (1981).

The BSA diffusivity was estimated to be 7×10^{-11} m^2/s (van den Berg and Smolders, 1989). Taylor et al. (1994) demonstrated that, because axial transport of protein was dominated by convection, the precise value of the diffusivity had little influence on the protein redistribution process. The transferrin diffusivity was, therefore, also taken to be 7×10^{-11} m^2/s.

Numerical solution

The coupled hydrodynamic and protein transport equations (Eqs. 1 and 5) were solved numerically by finite difference methods. The spatial derivatives in both equations were discretized using the control volume approach recommended by Patankar (1980). The time derivative in Eq. 5 was represented by a second-order accurate Crank-Nicolson scheme, while the diffusion and convection terms were handled by Patankar's (1980) "power law" scheme in order to prevent numerical instabilities caused by high local Peclet numbers. The Neumann boundary conditions required by Eq. 5 were incorporated by integrating over half control volumes (Patankar, 1980).

Starting with the initial ECS protein concentration, osmotic pressures were calculated using Eq. 9. The axial concentration gradient required for Eq. 1 was obtained by analytical differentiation of the cubic splines fitted to the ECS protein concentration profile. Once Eq. 1 was solved, the radially-averaged axial ECS velocities, midway between the grid locations (required for the "power law" scheme), were obtained by linear interpolation. The ECS protein concentrations at the next time step were then calculated by solving Eq. 5. The sequence of steps outlined above was then repeated for each subsequent

time step. Since the protein distribution did not change significantly over a single time increment, the ECS velocity solution was effectively lagged one step behind the concentration solution. Steady state was assumed to be achieved when the maximum protein concentration change between two successive time steps was less than 10^{-5} g/L. For the flow cycling simulations, the sign of the lumen inlet velocity $\bar{u}_{Li}$, appearing in Eq. 1, was reversed at regular intervals.

Materials and Methods

Hollow fiber cartridges

GFE-15 hollow-fiber cartridges (Gambro Dialysatoren, Hechingen, Germany) containing regenerated cellulose (Cuprophan) fibers were used. The molecular weight cutoff of the ultrafiltration membranes (90% rejection) was 18 kDa. To measure the dry fiber radii, fibers were chopped into 2-cm pieces using a surgical knife and were placed on a microscope slide without a coverslip. An optical microscope (Leitz Wetzlar, Germany) fitted with a lens containing a calibrated scale was used to measure the inner and outer radii of the transparent fibers. The radii were calculated from the averages of measurements on 20 fibers. The same procedure was followed for measuring the wet fiber outer radius, except that in this case two-three drops of water were added to wet the fibers. To check if the direction of wetting influenced the results, water was also added to the lumens of some fibers through syringe needles attached to the fiber ends. It was assumed that the swelling behavior of the fibers in cell culture medium would be similar to that in water.

The fiber inner and outer radii in the potting (the end region where the fibers are embedded in epoxy) were calculated from the average of microscopic measurements on 30 fibers. The dry permeable fiber length was determined as the distance between the potted end regions. Single fibers were measured dry and wet to determine the length increase upon wetting. A total number of 8,128 fibers were counted in a Gambro GFE-15 cartridge.

Lumen and ECS pressure measurements

To measure the lumen pressure drop as well as any radial pressure variations within the lumen manifolds (Figure 1), syringe needles (22 gauge) attached to water manometers, were inserted at different locations in both the upstream and downstream lumen manifolds. The ECS pressure drop was measured by connecting the two ECS ports to a manometer.

Membrane permeability measurement

The membrane permeability was determined by measuring the ECS permeate flow at different lumen pressures. The lumen inlet port was connected to a constant level water tank, the lumen outlet port was closed, and both ECS outlet ports were opened. The ECS pressure (P_E) was assumed to be atmospheric. The lumen pressure was measured near the radial center of the inlet (P_i) and outlet (P_o) lumen manifolds as described above. The transmembrane pressure driving force ΔP was calculated from the average value

$$\Delta P = (P_i + P_o)/2 - P_E. \tag{10}$$

It was assumed that all the measured pressure drop occurred across the membrane. This assumption was reasonable since the measured volumetric ECS flow rates were extremely low (maximum 6 mL/min) and hence both the lumen and ECS axial pressure drops were negligible. The membrane permeability L_p was calculated from the relationship between the ECS permeate flow rate Q and the transmembrane pressure:

$$Q = \frac{L_p}{\mu} A \Delta P \tag{11}$$

where A is the total membrane surface area based on the wet fiber inner radius.

HFBR protein distribution

Before each experiment, a sterile cartridge was pretreated by circulating phosphate-buffered saline (PBS) at a flow rate of 5 mL/s through the ECS with both lumen ports closed. This pretreatment was carried out for 3 h, with hourly PBS replacements. The lumen was then filled with PBS.

At the beginning of the protein distribution experiments, a solution of human transferrin (Gibco, Grand Island, NY) and/or BSA (Sigma Chemicals, St. Louis, MO) was circulated through the ECS at 5 mL/s for 15 min to obtain a uniform initial ECS protein concentration. For the unidirectional lumen flow experiments, the reactors were then operated in a vertical orientation with a downward lumen flow of 10 mL/s. This configuration was selected in order to eliminate potential natural convection effects due to density variations in the ECS (Piret and Cooney, 1990). Unless stated otherwise, these experiments were run for one week to obtain steady-state protein distributions. Sodium azide (0.2%) was added to all solutions to inhibit microbial growth.

The protein distributions were determined using the freeze-sectioning procedure developed by Piret and Cooney (1991). At the end of the experiment, the lumen liquid was displaced by pumped air. The cartridges were then rapidly immersed in liquid nitrogen. After storage at -70°C for less than a week, the cartridges were cut transversely into sections, each of which was weighed and thawed in 10–20-mL PBS for protein analysis. In control experiments using azoalbumin (sigma) we mapped the boundary between the protein-free region of the ECS and the polarized-albumin region (red) by observations made through the cartridge wall. This boundary did not shift from before to after freezing the cartridge.

Patkar et al. (1993) have reported BSA and transferrin adsorption on polysulfone fiber membranes, as well as transmembrane transferrin leakage in HFBRs. For the regenerated cellulose HFBRs used in this study, adsorption and transmembrane leakage of BSA and transferrin were undetectable. In all the experiments, between 92 and 98% of the initially added proteins were recovered from the cut reactor sections. Some of this protein was present in the two ECS ports and in small regions outside the potting (about 5 mL) at both reactor ends. In the discussion of experimental and modeling results, these regions were not considered to be part of the ECS, and the "initial" protein loadings were taken to be the average concentrations based on the amount of proteins recovered from the cut sections at the termination of each experiment.

Protein concentration measurements

Human transferrin was analyzed by a particle-based immunofluorescence assay using a Pandex fluorescent concentration analyzer (Baxter/Pandex, Mundelein, IL), as described by Patkar et al. (1993). BSA concentrations were determined using a protein assay kit based on color change of Coomassie Blue G-250 (Bio-Rad, Mississauga, ONT). All samples and standards were assayed in triplicates. The error bars in the figures denote 90% confidence intervals calculated from the standard errors in the assay results.

Results and Discussion

Fiber geometry, permeability and pressure measurements

The average inner and outer fiber radii in the potting section were about 10% smaller than the values measured for the dry fibers in the bundle (Table 1). This may have been caused during manufacture by the swelling of the epoxy as it set. Wetting was found to increase the permeable (nonpotted) fiber dimensions. The outer radius of the wet fibers was about 15% greater than that of the dry fibers. After wetting, the fiber length increased by approximately 10%. Optical effects introduced by the presence of water made it difficult to measure the wet fiber inner radii. Since the fibers were isotropic, the percent increase in fiber thickness was assumed to be equal to the percent increase in the fiber length. Thus, the wet fiber thickness was assumed to be 10% larger than the dry fiber thickness, yielding by difference, the wet fiber inner radius (Table 1).

The Krogh cylinder radius was calculated assuming a homogeneous fiber distribution in a cartridge with a constant inner shell diameter of 3.15 cm. The cylindrical cartridge shell diameter increased radially to 4.12 cm over a length of 2.1 cm at each end of the HFBR (Figure 1). The effect of these additional spaces on the ECS hydrodynamics and protein redistribution cannot be accounted for by the Krogh cylinder assumption and will be discussed when comparing the experimental data with the model predictions.

At a lumen water flow rate of 10 mL/s and in the absence of ECS proteins, the measured lumen pressure drop was 4,910 Pa. The overall lumen pressure drop was the sum of the pressure drops across the permeable and the two potted regions of the fiber bundle. Using the hydrodynamic model developed by Taylor et al. (1994) for the permeable region and the Hagen-Poiseuille equation for the two potted regions, an overall lumen pressure drop of 4,880 Pa was calculated. The measured ECS pressure under these conditions was 2,460 Pa, while the pressure drop between the upstream and downstream ECS ports was not detectable (<10 Pa). The model predicted that the average ECS pressure was exactly half of the upstream lumen pressure (2,440 Pa) and that the ECS pressure drop was 1.3 Pa. The agreement between all of the measured and predicted pressure results not only helped validate the hydrodynamic part of the model, but also suggested that the assumptions made in estimating the wet fiber inner radius were reasonable.

Use of the Krogh cylinder as a representative unit for all fibers in the bundle implied that each fiber lumen experienced the same flow rate, that is, radial pressure gradients in the lumen inlet and outlet manifolds were negligible. Park and Chang (1986) reported substantial radial pressure variations

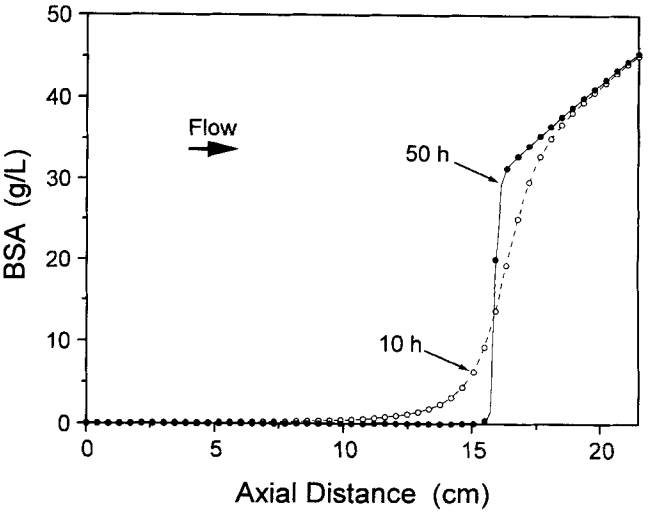

Figure 3. Comparison of 1-D and 2-D model simulations at BSA loading of 10 g/L.

(- -) 2-D model at 10 h; (—) 2-D model at 50 h; (o) 1-D model at 10 h; (•) 1-D model at 50 h.

in the lumen manifolds (Figure 1) for some HFBR geometries and operating conditions. The maximum measured pressure difference between the manifold center and circumference was 20 Pa, which was only 0.4% of the total lumen pressure drop. This indicated that all the fibers in the bundle were subject to approximately the same axial pressure drop regardless of their radial position.

The permeability measurements yielded a linear relationship between permeate flow rate and transmembrane pressure for lumen inlet pressures from 550 to 1,250 Pa. The calculated membrane permeability was $6 \pm 1 \times 10^{-15}$ m.

Validity of one-dimensional approximation

In contrast to the 2-D model of Taylor et al. (1994), the simpler 1-D model developed here neglects ECS and lumen radial gradients in velocities, pressures, and concentrations. Figure 3 compares the radially-averaged axial protein concentration profiles predicted by both models after 10- and 50-h operation at a lumen flow rate of 10 mL/s. The two profiles were virtually identical, indicating the validity of the one-dimensional assumption. Since the 1-D model required considerably less computational effort, it was used for all further simulations.

Transferrin polarization at low protein loading

Piret and Cooney (1990) observed extreme downstream polarization of transferrin and antibody in unidirectionally operated HFBRs. To check the extent of this phenomenon in Gambro reactors, ECS transferrin distributions were measured experimentally at low tranferrin loadings. These experiments, along with the high protein loading and flow-cycling experiments described later, provided a basis for validating the predictions of the 1-D model.

A cartridge loaded with 0.028-g/L transferrin was sacrificed after 2 h of unidirectional lumen flow at 10 mL/s. At this time, the steady-state protein distribution was not established, but downstream transferrin polarization was already signifi-

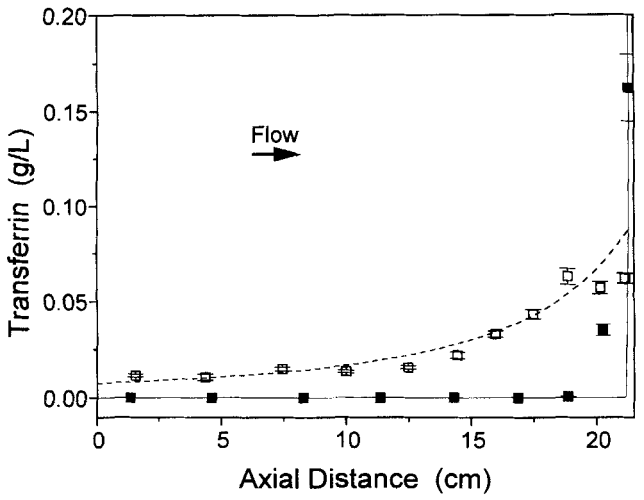

Figure 4. Transferrin distribution at low protein loading.

(□) Experiment after 2 h at 0.028 g/L transferrin; (■) experiment with 0.019 g/L transferrin at 4 days; (- -) model after 2 h; (—) model at 4 days. In Figures 4-8, the measured protein concentration of each frozen section is plotted at the axial midpoint of that section.

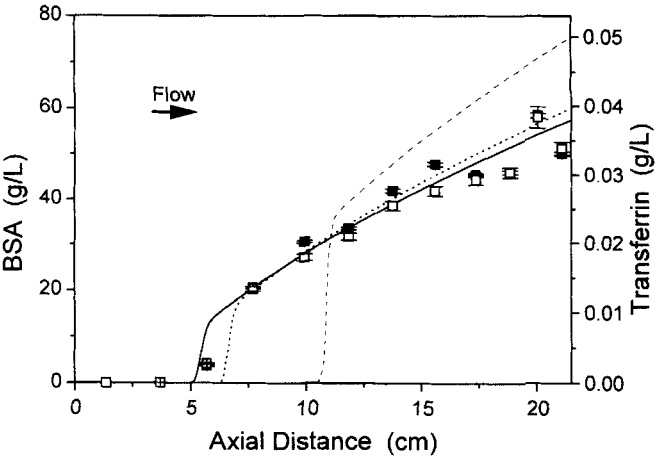

Figure 5. BSA and transferrin distributions after 1 week of unidirectional operation at 29-g/L BSA and 0.019-g/L transferrin loading.

(□) Experimental transferrin data; (■) experimental BSA data; (—) model simulation with wet fiber radius and dry fiber length; (- -) model simulation with dry fiber radius and length; (····) model simulation with wet fiber radius and length. The BSA axis scale was adjusted so that model lines for BSA and transferrin were identical.

cant (Figure 4). In the upstream 15-cm region of the ECS, the transferrin concentration was less than 0.02 g/L. Over the next 3 cm, the transferrin concentration increased monotonically to about 0.065 g/L, but fell slightly over the final 2 cm. Another experiment was performed with a 0.019-g/L transferrin loading and the HFBR was sacrificed after 4 days of 10-mL/s lumen recycle flow. The results, also shown in Figure 4, revealed a drastic downstream transferrin polarization. In the upstream 95% of the ECS, transferrin was not detectable ($< 3 \times 10^{-5}$ g/L), while at the downstream end, its concentration increased to about 0.16 g/L.

As can be seen from Figure 4, the agreement between the model predictions and the experimental results was quite good for both experiments. For the 2-h run, the model predicted a higher protein concentration at the downstream end than was actually observed. At 4 days, the model predicted an extreme protein polarization, but the measured transferrin distribution extended further upstream than was simulated. These discrepancies were believed to be due to the ECS manifolds. Over a 2-cm region at the upstream and downstream ends of the ECS, the cartridge shell diameter is expanded to create annular manifolds which are connected to the two ECS ports (Figure 1) and which do not contain fibers. These manifolds (each 9% of the total ECS volume) are relatively inaccessible to the secondary convective flows that occur around the fibers. Protein transport between these manifolds and the fiber bundle region of the ECS was therefore very slow. Thus, transferrin trapped in the downstream manifold, which was not segregated from the fiber bundle during the freeze-sectioning procedure, would have reduced the local average concentration in the case of the 2-h experiment and caused the 4 day profile to shift upstream.

Transferrin mediates iron uptake by cells and is thus an important constituent of most cell culture media. The extreme downstream transferrin polarization observed at low ECS protein loading is therefore expected to decrease upstream cell growth in HFBRs. Piret and Cooney (1990) demonstrated that downstream protein polarization in HFBRs can result in polarized hybridoma growth and decreased reactor antibody productivity. Thus, there is a need to develop alternative startup strategies to improve the distribution of proteins in the ECS.

Effect of high protein loading

One way to reduce transferrin polarization is to use relatively high initial concentrations of an inert, but osmotically active, protein such as BSA (Taylor et al., 1994). At 29-g/L BSA and 0.019-g/L transferrin loading, significantly less steady-state polarization of BSA and transferrin was observed (Figure 5). The BSA and transferrin were cleared from the upstream 5-cm region of the reactor. The protein concentrations increased rapidly over the next 4 cm, after which the increase was more gradual. The measured BSA profiles were similar to those described by Taylor et al.

The effect of high protein loading on protein distribution can be qualitatively explained. The secondary flow in the ECS drives the proteins to the downstream end. As the proteins accumulate, increasing osmotic pressures decrease the transmembrane flows in the downstream region, until at steady state, the flow is almost completely shut down. The resulting steady-state protein profile generally divides the ECS into two regions: an upstream region where the protein concentration is zero and convective secondary flow is present, and a downstream region which is essentially stagnant with an almost zero transmembrane flow (Taylor et al.) and a protein profile which increases monotonically with axial distance.

A quantitative description of this phenomenon is provided by the model equations described earlier. The solid line in Figure 5 shows the predicted BSA profile obtained using the wet fiber radii and the dry fiber length. It was found that the model predictions were influenced by the fiber dimensions. For example, the dashed line in Figure 5 was obtained using the dry fiber radii and length. The predicted BSA concentration profile was quite different from the observed experimental data, because for a given flow rate the lumen axial pressure

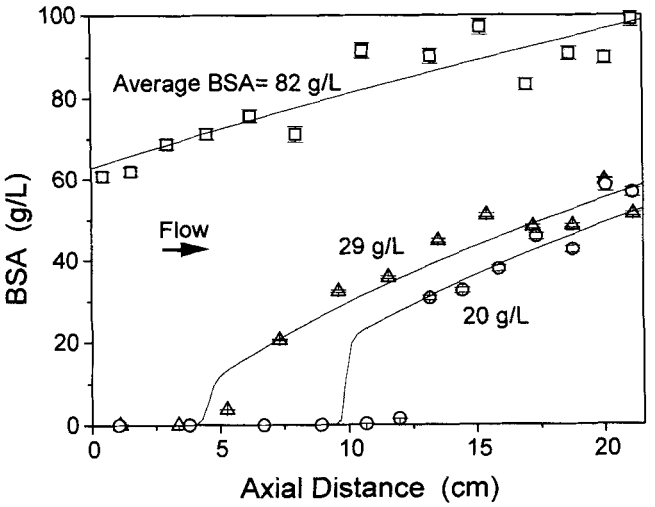

Figure 6. Effect of initial BSA loading (20-82 g/L) on BSA distribution.

The points denote experimental data and the lines show model simulations.

drop depends approximately on the fourth power of the fiber inner radius (Eq. 14); the lumen pressure gradient dictates the shape of the steady-state protein concentration profile (Taylor et al., 1994). Because the potted ends were fixed, the 10% length increase due to wetting caused the fibers in the cartridge to assume a wavy appearance. Consequently, the ECS volume was further reduced and the Krogh cylinder approximation became less accurate. Assuming that the axial expansion of the fibers resulted in a corresponding 10% increase in the lumen pressure drop, the model yielded the dotted line in Figure 5. Both the solid and dotted lines adequately matched the experimental results. Thus, because the axial expansion of the fibers can only be approximated by the model, all subsequent simulations were carried out using the wet fiber radii and the dry fiber length.

Figures 6 and 7 show the experimental steady-state concentration profiles of BSA and transferrin, respectively, at BSA loadings from 20 to 82 g/L, for a constant initial transferrin concentration of about 0.02 g/L. As the BSA loading was increased, both concentration profiles extended further upstream. At the highest loading, the BSA and transferrin concentration profiles occupied the entire length of the ECS. Thus, higher initial protein loading resulted in a more uniform ECS protein distribution. After the initial startup period, once the cells have grown to fill the ECS, the HFBR can then be operated with low ECS protein concentrations to facilitate protein product recovery. Comparison of the experimental and model predicted BSA distributions in Figure 6 indicated good agreement for all BSA loadings employed. The differences between the model and experimental results are probably mainly due to the nonideal geometry of the HFBR cartridge.

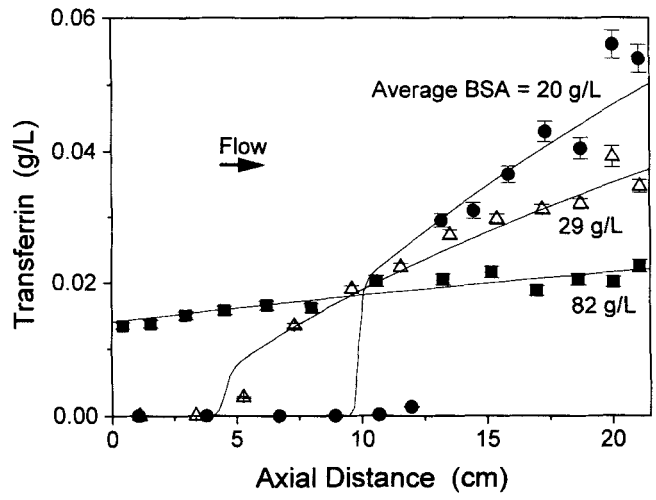

Figure 7. Effect of initial BSA loading (20-82 g/L) on transferrin distribution.

The average ECS transferrin concentration in each experiment was about 0.02 g/L. The points denote experimental data and the lines show model simulations.

One interesting observation made evident by Figures 5-7 was that, for a given BSA loading, the concentration profiles of BSA and transferrin were very similar. This phenomenon can be explained by considering the average ECS Peclet number for axial protein transport,

$$Pe = \frac{\overline{u}_E L}{D} \cong \frac{10^{-6} \times 0.215}{7 \times 10^{-11}} \cong 3{,}000. \tag{12}$$

These high Peclet numbers indicated that convection dominated diffusion as the primary mechanism of axial protein transport in the ECS. Since convection affected BSA and transferrin equally, it gave rise to similar concentration profiles. In fact, as long as the transferrin concentration was much less everywhere than the BSA concentration, such that the osmotic pressure due to transferrin had a negligible influence on the transmembrane flow, the model could be used to compute the transferrin profiles (Figure 7) from the predicted BSA profiles as:

$$\overline{C}_{\text{trans}}(z) = \overline{C}_{\text{BSA}}(z)\, \frac{\overline{C}_{\text{trans},0}}{\overline{C}_{\text{BSA},0}}, \tag{13}$$

where $\overline{C}_{\text{trans}}$ and $\overline{C}_{\text{BSA}}$ are radially-averaged transferrin and BSA concentrations, respectively; the subscript 0 refers to the initial uniform ECS concentration. Equation 13 also assumes that the transferrin distribution is "quasi-steady," that is, achieved shortly after the steady-state BSA profile has been established but before further differentiation of the two protein species can take place by diffusion. The similar close agreement between the experimental and predicted transferrin distributions in Figure 7 attests to the efficacy of Eq. 13.

Flow cycling

Periodic reversal of the lumen flow direction can result in a more uniform protein distribution because each such change reverses the direction of ECS protein transport. Piret and Cooney (1990) have shown experimentally that this approach resulted in a more uniform transferrin distribution as well as increased cell growth and reactor productivity.

To test the applicability of lumen flow cycling to the HFBRs used in this study, the lumen flow direction was reversed every hour in a horizontally oriented cartridge with an initial protein loading of 4.9-g/L BSA and 0.018-g/L transferrin. The reactor was operated for 4 days at 10 mL/s lumen flow and then

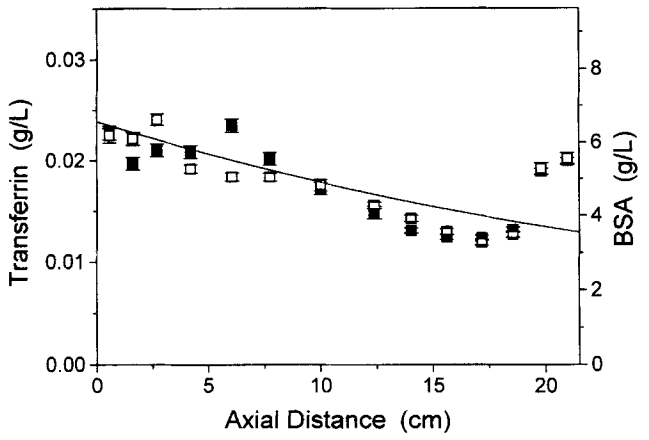

Figure 8. Model simulations vs. experimental data for flow-cycling run with a flow-switching time of 1 h for 4 d at initial loading of 4.9-g/L BSA and 0.018-g/L transferrin.

The points represent experimental data and the line denotes model simulation. The BSA axis scale was adjusted so that model lines for BSA and transferrin were identical.

sacrificed. Figure 8 demonstrates the utility of flow cycling in reducing downstream protein polarization. As the reactor was sacrificed at the end of the reverse flow cycle, both BSA and transferrin were polarized slightly towards the left end. As in the high protein loading experiments, the profiles of BSA and transferrin were very similar. However, the polarization was considerably less severe than was observed at steady state for the unidirectional operation shown in Figure 4.

Piret and Cooney (1990) observed that polarization of proteins increased the density of the solution in the downstream end of the ECS. This resulted in bulk sedimentation of the concentration protein solution within horizontal HFBRs operated with unidirectional lumen flow. To investigate the extent of this phenomenon, two sections at each ECS end were further divided into bottom and top halves. The concentrations of BSA and transferrin were 10–90% higher in the bottom section, thus demonstrating that after only 4 days of operation significant sedimentation of protein solutions had occurred even with flow cycling.

Also shown in Figure 8 are the model-predicted BSA and transferrin distributions for the flow cycling experiment. The agreement between theory and experiment was very good except near the right end, where the model predicted a lower protein concentration than was observed. This discrepancy can be explained qualitatively as follows. During the period of reverse lumen flow, although the proteins in the fiber bundle were convectively driven towards the left end, protein exchange between the fiber bundle and the relatively stagnant ECS manifold (Figure 1) was much slower than the convective transport in the fiber bundle. A higher protein concentration in the manifolds resulted in a higher average protein concentration in the right-end sections.

The generally excellent agreement between the model simulations and the experimental protein distribution results for a variety of situations (transient, steady-state and flow-cycling), we believe, successfully validated the theory. The model was then used with reasonable confidence to predict HFBR protein distributions for other operating conditions of interest.

Prediction of the critical protein loading

To implement the protein-loading strategy in any HFBR, it would be advantageous to know the critical protein loading above which the steady-state protein profiles, and thus the growth factor distributions, extend over the full length of the ECS. Here the steady-state model described by Taylor et al. (1994) was extended to allow an estimate of this critical concentration as a function of the lumen pressure drop.

Because of the typically low membrane permeabilities of ultrafiltration HFBRs, it is reasonable to assume that the lumen hydrostatic pressure $[\overline{P}_L(z)]$ falls linearly with axial distance and that the ECS hydrostatic pressure $[\overline{P}_E(z)]$ is virtually constant (Taylor et al.). At the critical protein loading, there is just sufficient protein to fill the ECS such that the transmembrane flow over the entire length of the reactor is essentially zero at steady state: $\overline{C}_E = 0$ at $z = 0$ and $P_E(z) - \overline{\Pi}_E(z) = \overline{P}_L(z)$. These two requirements imply that the ECS hydrostatic pressure is equal to the inlet lumen pressure and hence, according to the Hagen-Poiseuille equation:

$$\overline{P}_E = P_{Li} = \frac{8\mu L \overline{u}_{Li}}{r_1^2} = \frac{8\mu L Q}{\pi N r_1^4}, \tag{14}$$

where the downstream lumen pressure is assumed to be zero, without loss of generality. Here, Q is the lumen inlet flow rate and N is the number of fibers in the bundle. The critical initial concentration, C_{E0}^{crit}, can now be determined as:

$$C_{E0}^{\text{crit}} = \frac{1}{L}\int_0^L \overline{C}_E(z)\,dz \tag{15}$$

Since $\Pi(C)$ is a single-valued function of C, it can be inverted as $C = C(\Pi)$. Furthermore, since $\overline{\Pi}_E(z) = \overline{P}_E - \overline{P}_L(z) = P_{Li}z/L$, we can now change the integration variable to $\overline{\Pi}_E$,

$$C_{E0}^{\text{crit}} = \frac{1}{P_{Li}}\int_0^{P_{Li}} \overline{C}_E(\overline{\Pi}_E)\,d\overline{\Pi}_E. \tag{16}$$

Thus, the critical concentration is only a function of the lumen pressure drop and the osmotic pressure relationship $C(\Pi)$. For example, if BSA (< 100 g/L) is used to increase the ECS osmotic pressure, then

$$C_{E0}^{\text{crit}} = 0.012\,P_{Li} + 8.286\times10^{-7}P_{Li}^2 + 3.362\times10^{-11}P_{Li}^3 \tag{17}$$

where the constant coefficients were obtained by fitting a polynomial representation of $C(\Pi)$ to the BSA osmotic pressure data of Scatchard et al. (1946a,b). For the HFBRs used in this study at a lumen flow rate of 10 mL/s, the lumen pressure drop would be 3,850 Pa, and a BSA loading of 36 g/L would be required to extend the protein profile over the whole of the ECS. Although serum contains about 40-g/L BSA, it is possible that at high BSA concentrations some cell lines could experience low growth rates and/or low productivities. In addition, it may be desirable to reduce the BSA level to increase the purity of the recovered protein product. One way to reduce the critical protein loading during HFBR startup would be to decrease the lumen flow rate, thus decreasing the lumen pressure drop. Thus, for example, at a flow rate of 2.5 mL/s, the lumen pressure drop would be 960 Pa, and a BSA loading of

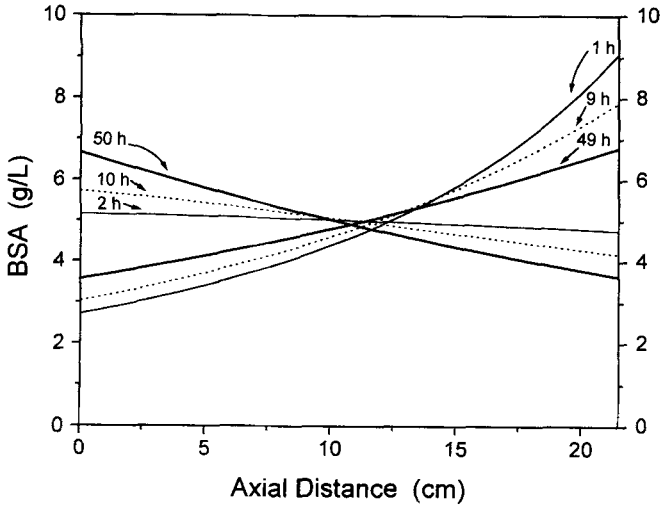

Figure 9. Transients for the flow-cycling experiment at a membrane permeability of 6×10^{-15} m, 5-g/L BSA loading and 1-h flow-switching time.

Note that all lines represent BSA distribution at times when flow direction was reversed.

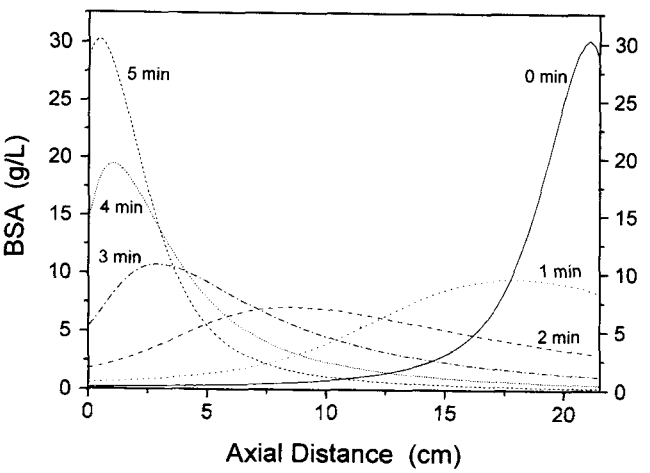

Figure 10. Protein concentration profiles during a single half cycle at a membrane permeability of 6×10^{-13} m, 5-g/L BSA loading, and 5-min flow-switching time.

only 11 g/L would be sufficient. Slower flow rates, however, could limit the oxygen transport to the immobilized cells. Calculations made using the effectiveness factors and the equations derived by Piret and Cooney (1991) could be used to ensure minimal oxygen limitations in the ECS.

Flow cycling simulations

A problem in experiments with HFBRs is that it is difficult to determine protein concentrations noninvasively. Thus experiments to measure the evolution of the protein concentration profiles before steady state is reached would require many reactors to be sacrificed after different times of operation. The mathematical model developed here can be used with reasonable confidence to predict these transients.

Transients corresponding to the 1-h flow cycling experiment were computed using the 1-D model, starting from an initial uniform ECS BSA concentration of 5 g/L. After about 50 h of operation, the profiles obtained at the end of each half cycle were mirror images of each other (Figure 9).

Fiber membrane permeability also affects this steadily oscillating protein distribution. Asymmetric polysulfone membranes typically have a 100-fold higher permeability (Patkar et al., 1993) than the regenerated cellulose membranes used in this study, that is, 6×10^{-13} vs. 6×10^{-15} m, respectively. For the higher permeability membranes, a flow-switching time of 1 h resulted in extreme protein polarization. Simulations were therefore performed at a switching time of 5 min. BSA concentration profiles generated at different times for a single half cycle, after the condition of steady oscillation was established, are shown in Figure 10. It is interesting to note that the roughly bell-shaped BSA profiles occurring at intermediate times in the half cycle were similar to the protein concentration profile reported by Piret and Cooney (1990) in a polysulfone membrane HFBR with an average ECS cell concentration of 10^7 cells/mL.

The flow-switching time is an important variable that determines the relative uniformity of the steadily oscillating protein distribution. Figure 11 shows the end-of-cycle BSA distributions obtained at switching times of 1–10 h for an initial concentration of 5 g/L and a membrane permeability of 6×10^{-15} m. As expected, the protein distributions became less uniform as the switching time increased. The switching time of 1 h resulted in a relatively uniform protein concentration throughout the ECS, whereas a 10 h switching time led to intermittent very low protein concentrations in the upstream 75% of the ECS.

Conclusions

HFBRs, operated with unidirectional flow and low protein loadings, suffer from extreme downstream polarization of growth factor proteins. In the absence of BSA addition, significant downstream polarization of transferrin was observed after 2 h of unidirectional operation. At steady state, only

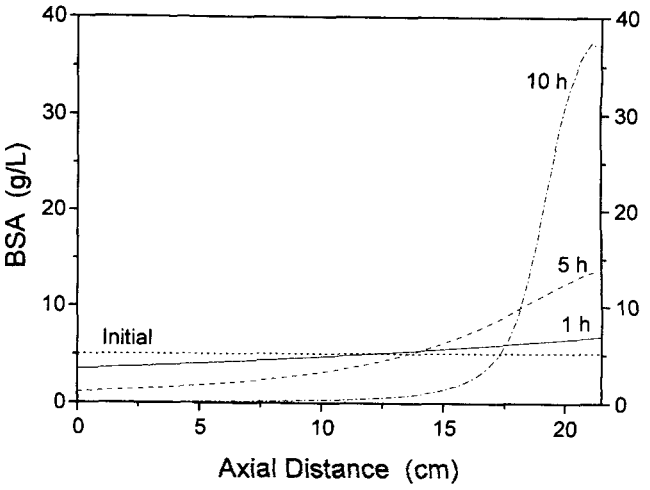

Figure 11. Initial uniform distribution and effect of flow-switching time on steady-state BSA distribution at the end of the forward cycle at 5-g/L BSA loading and membrane permeability of 6×10^{-15} m.

about 5% of the ECS contained measurable levels of transferrin. It is expected that reactors operated in this fashion would support cell growth only in the downstream ECS end, resulting in substantially lower productivity.

Two different strategies to improve the growth factor distribution were explored experimentally and theoretically. Higher BSA loading resulted in more uniform BSA and transferrin distributions. The concentration profiles of both proteins were very similar, indicating the dominance of convective over diffusive protein transport. At BSA loadings over 36 g/L, for the reactor and operating conditions considered here, the steady-state protein distributions should extend over the entire length of the ECS. Such high protein loadings only would be needed during the startup phase of HFBR operation when growth factors are required to promote cell growth. The effectiveness of the flow-cycling strategy reported by Piret and Cooney (1990) in counteracting protein polarization was also studied. For the HFBRs used in this study, switching of the lumen flow direction every hour resulted in a relatively uniform protein distribution. However, significant sedimentation of concentrated protein solution to the bottom of a horizontally oriented cartridge was observed after 4 days of operation.

A simple one-dimensional model was developed to describe the hydrodynamics and protein transport in HFBRs. This model was found to yield results virtually identical to those obtained using the more complicated 2-D model developed by Taylor et al. (1994). The model predictions showed good agreement with protein distributions obtained in transient, steady-state, and flow-switching experiments.

The 1-D model was used to investigate ECS protein redistribution in HFBRs. The simple steady-state model described by Taylor et al. was extended to determine the critical protein concentration needed for virtual stoppage of ECS flow. At this protein loading, the steady-state protein distribution would span the full length of the ECS. The critical loading was shown to depend only on the osmotic pressure relationship and the total lumen pressure drop. In particular, if BSA was used to increase the ECS osmotic pressure, a simple relationship between this critical concentration and the lumen inlet pressure was determined.

Periodic switching of flow direction is another method of improving growth factor distribution in HFBRs. To understand the protein transport in this mode of operation, simulations were performed at different membrane permeabilities and flow switching times. Under steadily oscillating conditions, the protein concentration profiles obtained at the end of the forward and reverse half flow cycles were mirror images. As expected, for membranes with higher permeability, shorter flow-switching times were required to obtain relatively uniform protein distribution throughout each flow cycle.

The model described here assumes that cells in the ECS do not offer a significant resistance to flow. This assumption will only be valid at the low cell concentrations encountered during reactor startup. Models to describe a reactor filled with cells are currently being developed. Also, our modeling approach, which has been validated for a conventional HFBR, can be applied to analyze the hydrodynamics and protein redistribution in a wider range of ultrafiltration membrane bioreactors. Such models could greatly assist in designing and optimizing the operation of potential new bioreactors.

Acknowledgment

This work was sponsored by the Natural Sciences and Engineering Research Council of Canada.

Notation

A = total fiber surface area based on wet fiber inner radius, m^2
C = protein concentration, g/L
$\overline{C}$ = radially-averaged protein concentration, g/L
C_{E0} = initial ECS protein concentration, g/L
C_{E0}^{crit} = critical initial protein concentration, g/L
D = protein diffusivity, m^2/s
L = fiber permeable length, m
L_p = membrane permeability, m
M = protein molecular weight, Da
N = number of fibers in HFBR
P = hydrostatic pressure, Pa
P_E = average ECS pressure, Pa
P_i = pressure in the upstream lumen manifold, Pa
P_{Li} = lumen inlet hydrostatic pressure, Pa
P_{Lo} = lumen outlet hydrostatic pressure, Pa
P_o = pressure in the downstream lumen manifold, Pa
ΔP = transmembrane hydrostatic pressure difference, Pa
Q = flow rate at the fiber bundle inlet, m^3/s
r_1, r_2, r_3 = fiber inner radius, outer radius and Krogh cylinder radius, m
R = universal gas constant, J/mol·K
t = time, s
T = absolute temperature, K
$\overline{u}$ = radially-averaged axial velocity, m/s
z = axial distance, m

Greek letters

μ = fluid viscosity, kg/m·s
Π = osmotic pressure, Pa
$\overline{\Pi}$ = radially-averaged osmotic pressure, Pa

Subscripts

E = extracapillary space (ECS)
i = lumen inlet
L = lumen
o = lumen outlet
trans = transferrin
0 = initial

Literature Cited

Altshuler, G. L., D. M. Dziewulski, J. A. Sowek, and G. Belfort, "Continuous Hybridoma Growth and Monoclonal Antibody Production in Hollow Fiber Reactors-Separators," *Biotechnol. Bioeng.*, **28**, 646 (1986).

Bruining, W. J., "A General Description of Flows and Pressures in Hollow Fiber Membrane Modules," *Chem. Eng. Sci.*, **44**, 1441 (1989).

David, G. S., R. A. Reisfeld, and T. H. Chino, "Continuous Production of Carcinoembryonic Antigen in Hollow Fiber Cell Culture Units," *J. Nat. Cancer Inst.*, **60**, 303 (1978).

Evans, T. L., and R. A. Miller, "Large-Scale Production of Murine Monoclonal Antibodies Using Hollow Fiber Bioreactors," *BioTechniques*, **6**, 762 (1988).

Heath, C. A., and G. Belfort, "Immobilization of Suspended Mammalian Cells: Analysis of Hollow Fiber and Microcapsule Bioreactors," *Adv. Biochem. Eng/Biotechnol.*, **34**, 1 (1987).

Heath, C. A., G. Belfort, B. E. Hammer, S. D. Mirer, and J. M. Pimbley, "Magnetic Resonance Imaging and Modeling of Flow in Hollow-Fiber Bioreactors," *AIChE J.*, **36**, 547 (1990).

Heifetz, A. H., J. A. Braatz, R. A. Wolfe, R. M. Barry, D. A. Miller, and B. A. Solomon, "Monoclonal Antibody Production in Hollow Fiber Bioreactors Using Serum-Free Medium," *BioTechniques*, **7**, 192 (1989).

Kelsey, L. J., M. R. Pillarella, and A. L. Zydney, "Theoretical Analysis of Convective Flow Profiles in a Hollow Fiber Membrane Bioreactor," *Chem. Eng. Sci.*, **45**, 3211 (1990).

Knazek, R. A., P. O. Kohler, and P. M. Gullino, "Hormone Production by Cells Grown *in vitro* on Artificial Capillaries," *Exp. Cell Res.*, **84**, 251 (1974).

Krogh, A., "The Number and Distribution of Capillaries in Muscles with Calculations of the Oxygen Pressure Head Necessary for Supplying the Tissue," *J. Physiol.*, **52**, 409 (1919).

Park, J. K., and H. N. Chang, "Flow Distribution in the Fiber Lumen Side of a Hollow-Fiber Module," *AIChE J.*, **32**, 1937 (1986).

Patankar, S. V., *Numerical Heat Transfer and Fluid Flow*, Hemisphere, New York (1980).

Patkar, A. Y., B. D. Bowen, and J. M. Piret, "Protein Adsorption to Polysulfone Membranes in Hollow Fiber Bioreactors Used for Serum-Free Mammalian Cell Culture," *Biotechnol. Bioeng.*, **42**, 1099 (1993).

Pillarella, M. R., and A. L. Zydney, "Theoretical Analysis of the Effect of Convective Flow on Solute Transport and Insulin Release in a Hollow Fiber Bioartificial Pancreas," *J. Biomech. Eng.*, **112**, 220 (1990).

Piret, J. M., and C. L. Cooney, "Mammalian Cell and Protein Distributions in Ultrafiltration Hollow Fiber Bioreactors," *Biotechnol. Bioeng.*, **36**, 902 (1990).

Piret, J. M., D. A. Devens, and C. L. Cooney, "Nutrient and Metabolite Gradients in Mammalian Cell Hollow Fiber Bioreactors," *Can. J. Chem. Eng.*, **69**, 421 (1991).

Piret, J. M., and C. L. Cooney, "Model of Oxygen Transport Limitations in Hollow Fiber Bioreactors," *Biotechnol. Bioeng.*, **37**, 80 (1991).

Nyberg, S. L., R. A. Shatford, M. V. Peshwa, J. G. White, F. B. Cerra, and W. S. Hu, "Evaluation of a Hepatocyte-Entrapment Hollow Fiber Bioreactor: a Potential Bioartificial Liver," *Biotechnol. Bioeng.*, **41**, 194 (1993).

Scatchard, G., A. C. Batchelder, and A. Brown, "Preparation and Properties of Serum and Plasma Proteins: VI. Osmotic Equilibria in Solutions of Serum Albumin and Sodium Chloride," *J. Amer. Chem. Soc.*, **68**, 2320 (1946a).

Scatchard, G., A. C. Batchelder, A. Brown, and M. Zosa, "Preparation and Properties of Serum and Plasma Proteins: VII. Osmotic Equilibria in Concentrated Solutions of Serum Albumin," *J. Amer. Chem. Soc.*, **68**, 2610 (1946b).

Taylor, D. G., J. M. Piret, and B. D. Bowen, "Protein Polarization in Isotropic Membrane Hollow-Fiber Bioreactors," *AIChE J.*, **40**(2), 321 (1994).

Tharakan, J. P., and P. C. Chau, "Operation and Pressure Distribution of Immobilized Cell Hollow Fiber Bioreactors," *Biotechnol. Bioeng.*, **28**, 1064 (1986).

Vilker, V. L., C. K. Colton, and K. A. Smith, "The Osmotic Pressure of Concentrated Protein Solutions: Effect of Concentration and pH of Saline Solutions of Bovine Serum Albumin," *J. Coll. Interf. Sci.*, **79**, 548 (1981).

von Wedel, R. J., "Mass Culture of Mouse and Human Hybridoma Cells in Hollow-Fiber Culture," *Commercial Production of Monoclonal Antibodies: A Guide for Scale-up*, S. S. Seaver, ed., Marcel Dekker, New York, p. 159 (1987).

Waterland, L. R., C. R. Robertson, and A. S. Michaels, "Enzyme Catalysis Using Asymmetric Hollow Fiber Membranes," *Chem. Eng. Comm.*, **2**, 37 (1975).

Manuscript received Sept. 8, 1993, and revision received Feb. 9, 1994.